OPEN ACCESS

University of BRISTOL

Capuzzi, M., Pirrera, A., & Weaver, P. M. (2015). Structural design of a novel aeroelastically tailored wind turbine blade. Thin-Walled Structures, 95, 7-15. DOI: 10.1016/j.tws.2015.06.006

Peer reviewed version

Link to published version (if available):
10.1016/j.tws.2015.06.006

Link to publication record in Explore Bristol Research
PDF-document

University of Bristol - Explore Bristol Research
General rights

Structural Design of a Novel Aeroelastically Tailored Wind Turbine Blade

M. Capuzzi*, A. Pirrera*, P.M. Weaver

*Advanced Composites Centre for Innovation and Science,
Department of Aerospace Engineering, University of Bristol, Queen's Building,
University Walk, Bristol BS8 1TR, UK*

Abstract

The structural design for a recently presented aeroelastically-tailored wind turbine blade is produced. Variable elastic twist has been shown to improve performance in response to load variation across different wind conditions. This load variation is exploited as a source of passive structural morphing. Therefore, the angle of attack varies along the blade and adjusts to different operating conditions, hence improving both energy harvesting and gust load alleviation capability, below and above rated wind speed, respectively. The twist variation is achieved by purposefully designing spatially varying bend-twist coupling into the structure via tow steering and using a curved blade planform. This process enables the blade sections to twist appropriately while bending flapwise.

To prove the feasibility of the proposed adaptive behaviour, a complete blade structure is analysed by using refined finite element models, with structural stability and strength constraints imposed under realistic load cases. Nonlinear structural effects are analysed as well as modal dynamic features. In addition, the weight penalty due to aeroelastic tailoring is assessed using structural optimisation studies.

Keywords: Aeroelastic tailoring, Wind turbine blade design, Tow steered laminates, Finite elements analysis, Adaptive structures

*Corresponding author
Email addresses:* `marco.capuzzi@bristol.ac.uk` (M. Capuzzi),
`alberto.pirrera@bristol.ac.uk` (A. Pirrera)

1. Introduction and background

In the context of advanced structural engineering, the expression "adaptive structure" is generally used to describe a construction that improves its performance by changing shape in response to an external stimulus. The adjective passive, as in "passive adaptive structure" is added to refer to a specific subset that utilises changes in the operating environment to facilitate the change in shape.

Passive designs have been investigated widely for Wind Turbine (WT) applications, as shown for instance in [1–6]. In [7] and [8] the authors presented a novel adaptive concept for a 45 m blade that was shown to simultaneously increase the yielded power and decrease the magnitude of gust-induced loads. These improvements are obtained with a distribution of bend-induced elastic twist that varies non-monotonically along the blade's span (see figure 1 for the distribution at the rated wind speed. At different wind speeds this distribution scales up or down but its general features are retained). By allowing elastic twist to be added to the blade's pre-twist and pitch, the overall aerodynamic twist matches the theoretical optimum more closely than conventional designs, thereby improving turbine power. Increasing flapwise bending loads causes a nose-down rotation of the blade. Thus, the resulting deformation also provides a reduction of the gust-induced loads. In [8], by means of a simple structural analysis, the novel induced twist distribution is designed into a blade, idealised as a spar (box section). The targeted adaptive behaviour is achieved by superimposing geometrical and material bend-twist couplings. Specifically, a curved planform provides geometric coupling, whereas unbalanced composite laminates provide the material coupling. Tow steering is exploited to change the amount of material coupling along the blade axis [9], herein defined as the curvilinear line lying on the rotor plane and passing through the quarter-chord point of cross-sections (see dashed line in figure 2).

In this article, the structural design of the recently proposed adaptive blade concept is further refined. The passive adaptive capability is designed into a reference blade, subject to conventional structural limitations. Strength allowables and buckling constraints are imposed. The weight penalty due to aeroelastic tailoring is also assessed. The final design, although not optimised, shows that the adaptive capability does not compromise structural integrity (i.e. strength, stability and stiffness).
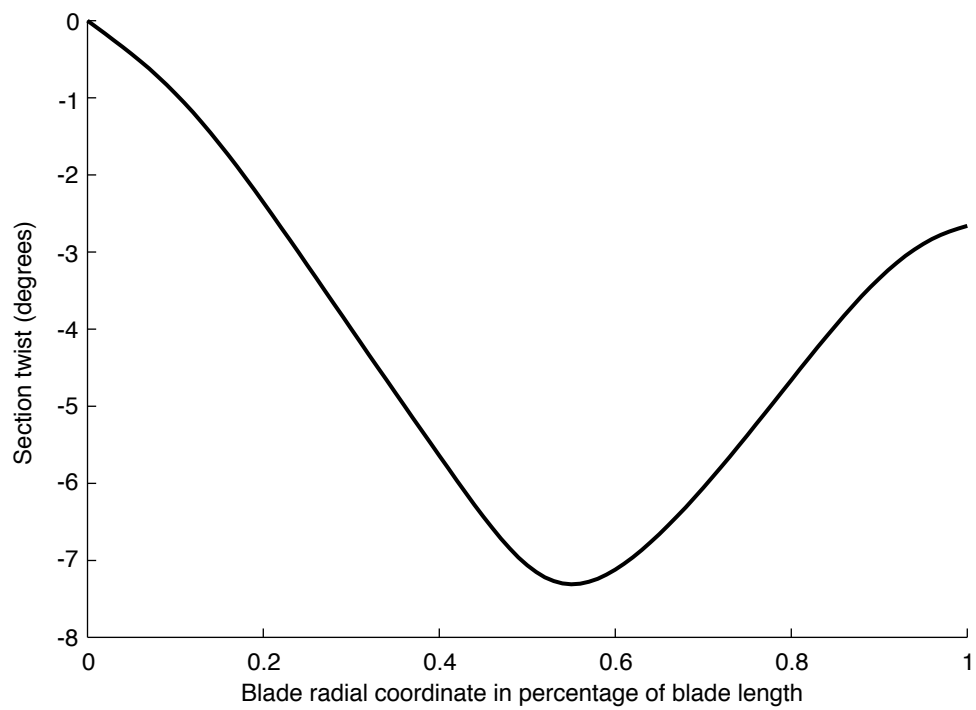
Figure 1: Target distribution of induced elastic twist under the aerodynamic load at rated wind condition

Table 1: Material properties, AS/3501 carbon-epoxy (transversally isotropic material).

E_{11} [GPa]	E_{22} [GPa]	ν_{12} [$-$]	G_{12} [GPa]	ρ [kg/m^3]
138	8.96	0.3	7.1	1600

2. Design of the adaptive spar

A spar that meets the intended adaptive behaviour and fulfils structural constraints is presented in this section. The concept's feasibility is assessed with a geometrically accurate structural model, thus improving on the analyses in [8] that were based on a two-node tapered composite beam finite element based upon work of Librescu [10]. Subsequently, the accompanying weight penalty due to stiffness tailoring is discussed.

2.1. Finite element analysis, functional design of the adaptive spar

The increase of modelling fidelity is not only achieved with a three dimensional finite element (FE) model (instead of anisotropic beam models), but also by using a more realistic geometry.

`CQUAD 4` NASTRAN plate FE and `PCOMP` properties capture tow steered laminate characteristics by varying the fibre orientation spanwise, over the caps of the spar box. The continuous fibre paths are approximated with a piecewise constant distribution over the plate elements. A mesh convergence analysis showed that 24 elements along the perimeter of the spar section and 300 elements spanwise were sufficiently accurate. The spar taper is modelled using a structured mesh that is increasingly refined towards the tip. The material properties are shown in Table 1.

The adaptive response is determined using the aerodynamic load distribution at the rated wind speed. Aerodynamic loads herein are calculated using a Blade Element Momentum model for steady state flow. The model is enhanced with tip and hub loss factors and the Buhl correction for the turbulent windmill state (for further details on the algorithm and aerodynamic mesh see [7]). The rated condition characterises the WT's operating range. Specifically, it corresponds to the lowest speed at which the power yielded is limited by the control system. The extreme load, used for strength and buckling analyses, is obtained by scaling the load distribution at rated. A scaling factor of 1.55 is used, because it ensures that the extreme condition for the flapwise bending moment at root is reached. This extreme value is

obtained from the design loads of the reference blade. The above-mentioned load results in bending of the blade out of the rotor plane, causing compression over the suction side of the structure. Linear buckling analyses are undertaken to check the global and local structural stability.

In this phase of the study, edgewise loads (bending of the blade within the rotor plane) have not been considered because the spar is not representative of the stiffness of the whole structure. Therefore, an edgewise load that drives the design of the spar, would be of secondary importance when the structural contribution of the skins is added.

The geometry of the spar is obtained by intersecting the blade's aerodynamic profile with two vertical walls (webs), both perpendicular to the rotor plane. The spar's width varies linearly from 40 cm to 10 cm with its cross sections centred at the blade's quarter-chord point towards the leading edge (LE). These values were obtained by adapting the results of the spar's structural optimisation presented in [11] and following engineering judgement. The latter being based on the observation, reported in the same article, that the structural performance is relatively insensitive to the spar's position within the aerodynamic section. The thickness of the walls is also sized according to the results in [11]. However, the caps' thickness and lay-up were later tailored to introduce the desired anisotropic elastic effects. Conversely, the webs are not tailored. Their stiffness should be appropriate to withstand edgewise loads, as imposed in the structural optimisation [11].

In [8] the targeted distribution of induced elastic twist is achieved by means of material and geometrical bend-twist coupling. The former is obtained by employing mirror-symmetric unbalanced laminates on the upper and bottom cap of the box section. The latter is achieved by exploiting the sections' off-set due to the swept planform of the blade. The unbalanced laminates used in this spar design are characterised by the fibre paths shown in figure 2. Specifically, 80% of the cap thickness is made of plies locally oriented as shown in the figure. The remaining portion is made of conventional lay-up orientations (i.e. $0, 90, \pm 45$ degrees). A minimum number of zero degrees plies is enforced, to ensure a global load path along the spar axis.

The curvilinear planform of the structure is obtained by imposing a linear variation in angle between the spar axis and the radial direction. The curve that defines the shape of the blade axis is obtained by integrating the tangent of this angle along the radial direction. Starting from the baseline geometry, each section of the spar is translated perpendicularly to the radial
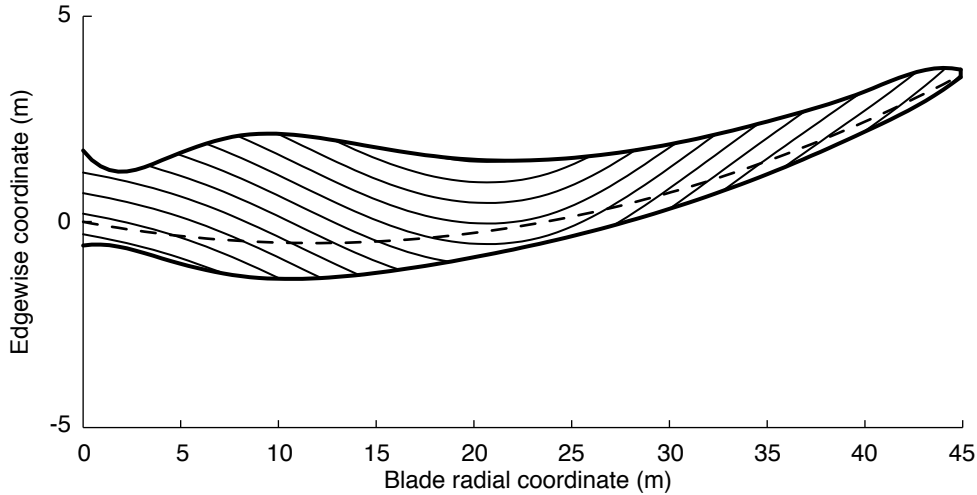
5

Figure 2: Steered fibre orientation along the blade (not to scale)

coordinate, to bring its centre onto the curved axis. Then, the section is also rotated around a direction perpendicular to the rotor plane. This rotation allows the profile to be perpendicular to the position vector connecting the section quarter-chord and rotor centre. Although, this is not the only method to define the curved blade geometry starting from its swept axis and its straight three-dimensional shape, it is convenient and follows simple concepts of rotor aerodynamics that are described in Appendix A. The angle between the blade axis and the radial direction is considered to vary between $-5 \deg$ at the root and $14 \deg$ at the tip. For reference, a positive rotation corresponds to a displacement of the section towards the trailing edge (TE). These angles result in a shape for the blade axis that has a maximum forward displacement of $0.52\,\text{m}$ at $12\,\text{m}$ of radial coordinate and $3.56\,\text{m}$ (8% of the blade length) of reverse displacement at the blade tip. By moving the inboard portion of the blade axis forward and then backward further outboard, the geometrically induced twist close to the blade's mid-span section is increased. Indeed, this shape of the planform increases the off-set of highly loaded sections, i.e. sections in the outermost half of the blade, with respect to the mid-span. On the other hand, to obtain the same off-set without bringing the first half of the structure forward, the displacement at the tip would have to be significantly increased. This consideration suggests higher angles are needed for the orientation of the blade axis in its outermost half,
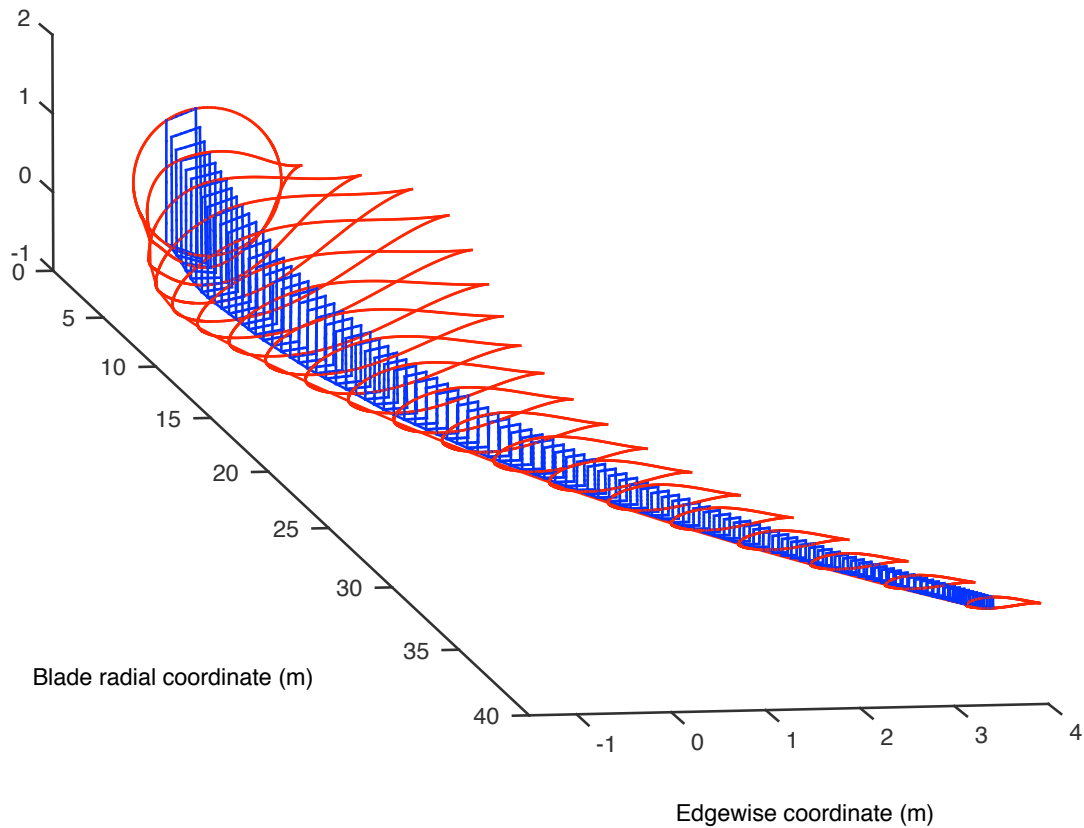
6

Figure 3: Spar's sections fitting the blade's aerodynamic profile

thus resulting in a planform shape more complex and, therefore, expensive to be manufactured and transported. For current purposes, the blade is treated as being aerodynamically straight. The reader is again referred to Appendix A for further details concerning the aerodynamics of curved blades.

In conclusion, the spar design fulfils the following requirements:

- the four corners of the box lie on the aerodynamic profile of the reference blade (as shown in figure 3);

- 80% of cap thickness is made of tailored plies, with the variable fibre orientation shown in figure 2. These fibre paths were introduced and justified in [8];

- under the aerodynamic load at the rated wind speed, the distribution

7

of the spar's induced elastic twist reproduces the targeted passive behaviour (as shown in figure 4);

- strain allowables and buckling loads are not reached at the extreme load, i.e. equivalent static gust;

- tower clearance, under the extreme flapwise load, is ensured. The limiting value of the reference blade (9.05 m) defines such a constraint and the extreme tip displacement for the proposed spar is found to be 7 m only; and

- the lay-ups of the walls guarantee a continuous load path, as a minimum number of zero degree plies is present in all of the walls. (Note, over the curved planform, ply angles are defined with respect to the local orientation of the blade axis. In other words, zero degrees plies are tow steered to remain parallel to the blade axis).

Figure 4 shows the elastic twist induced into the spar at the rated wind speed. The strain in the outermost ply is shown in figure 5, for the extreme static load. For reasons of brevity, linear buckling results are not shown. However, the minimum safety factor is found to be 1.29.

2.2. Weight penalty due to stiffness tailoring

In section 2.1, a spar design that realises the desired adaptive behaviour was presented. This design required tailoring of the elastic properties of the structure, with a consequent weight penalty in comparison to a structurally optimised blade.

In order to estimate the penalty, an additional adaptive spar of minimal weight is produced by repeating the structural optimisation described in [11]. The design space therein is now modified and narrowed. Specifically, 80% of the total cap thickness, which is a variable of the problem, is constrained to be made from plies oriented as shown in figure 2, where the maximum fibre skew angle is 15 deg inboard and 12 deg outboard. All other settings of the optimisation routine (i.e. constraints, load cases, objective function, structural modelling, etc.) are as reported in [11]. The objective function, which is minimised, is the weight of the spar cross-section, while the constraints impose that static strength and buckling allowables are not exceeded in each of the cross-section walls. A section-by-section optimisation is performed every
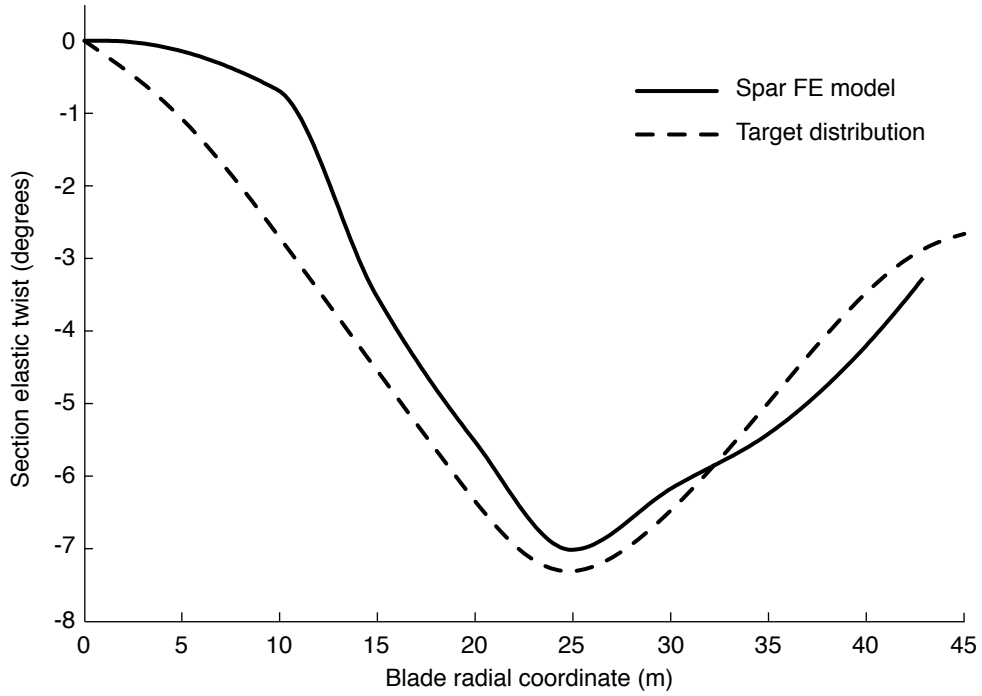
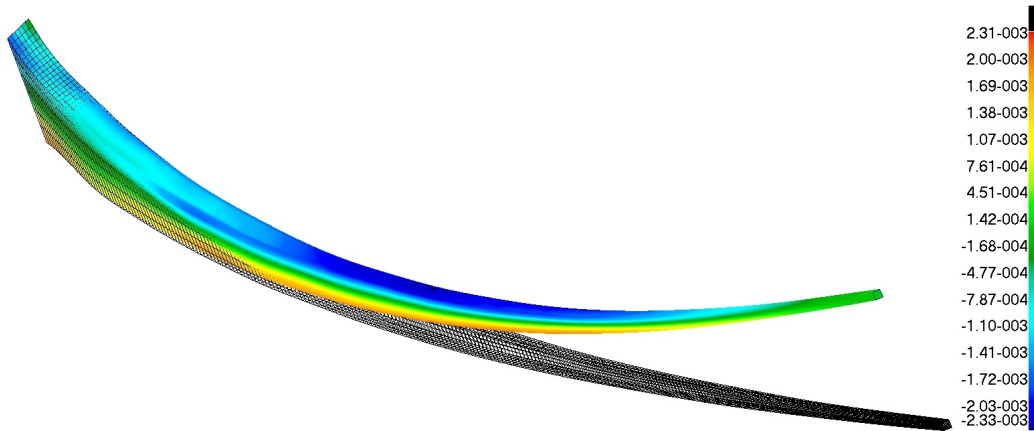Figure 4: Distribution of induced elastic twist under rated aerodynamic load, FE analysis results

Figure 5: Distribution of direct axial strain along the spar's radial coordinate

9

five metres along the blade span, thus involving nine sections over the 45 m blade.

It should be noted that this optimisation does not guarantee that the targeted adaptive behaviour is met. A more comprehensive optimisation study should include the adaptive capability as a second objective. It is also noted that the resulting spar design is probably oversized, i.e. it is not the lightest adaptive design possible. Indeed, in this study, the reference blade's extreme loads have been used, regardless of the fact that passive adaptive behaviour should reduce critical aerodynamic loads. An estimation of the gust load reduction would allow a more accurate evaluation of the weight penalty due to tailoring. In principle, when load reduction is accounted for, stiffness tailoring can also facilitate lighter structures. Nevertheless, the results herein are thought to provide a reasonable estimate for the weight penalty due to stiffness tailoring.

Figure 6 shows a section of the structurally optimised adaptive spar in comparison with the corresponding conventional layout from [11]. This figure shows that the optimiser recovers the stiffness lost due to tailoring by moving the section towards the LE, where the airfoil is thicker—a characteristic observed at all radial positions.

Figure 7 shows the distribution of mass along the blade span of both the spar with and without stiffness tailoring. Interestingly, despite the fact that the ply orientation over a set percentage of the cap thickness is pre-set to be less efficient, no significant increase in weight per unit length is observed. The total mass is calculated by integration along the blade length. Remarkably, the aeroelastically tailored spar is only 5.06% heavier than the structural optimum and is assumed to be a good estimate of the weight penalty due to elastic tailoring.

Figure 8 demonstrates the effect of structural optimisation on the design of the adaptive spar. The strain distribution is more uniform and, on average, closer to the allowables (3600 microstrain) than in the design shown in section 2.1. By comparing these two designs further, it is also noted that the optimised spar is wider closer to the root. Furthermore, when performing a linear buckling analysis, the minimum buckling safety factor is 1.09, as opposed to 1.29 for the initial adaptive design. Figure 9 shows the distribution of induced twist of the optimised spar under the aerodynamic load at rated wind speed. As a result of the optimisation study, the minimum value decreases in magnitude, but the targeted adaptive behaviour is retained. As anticipated, to obtain an optimised adaptive spar, the theoretical optimal
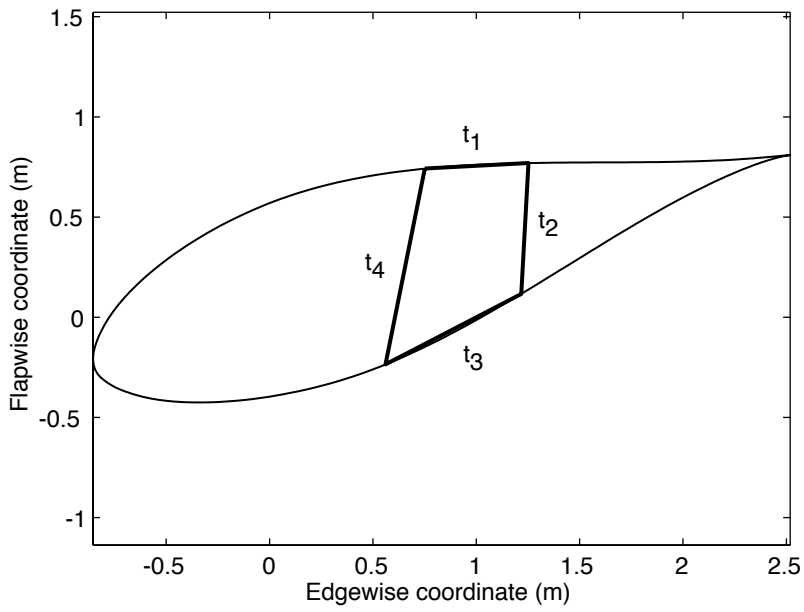
(a) Mass $= 111.69\,\mathrm{kg/m}$
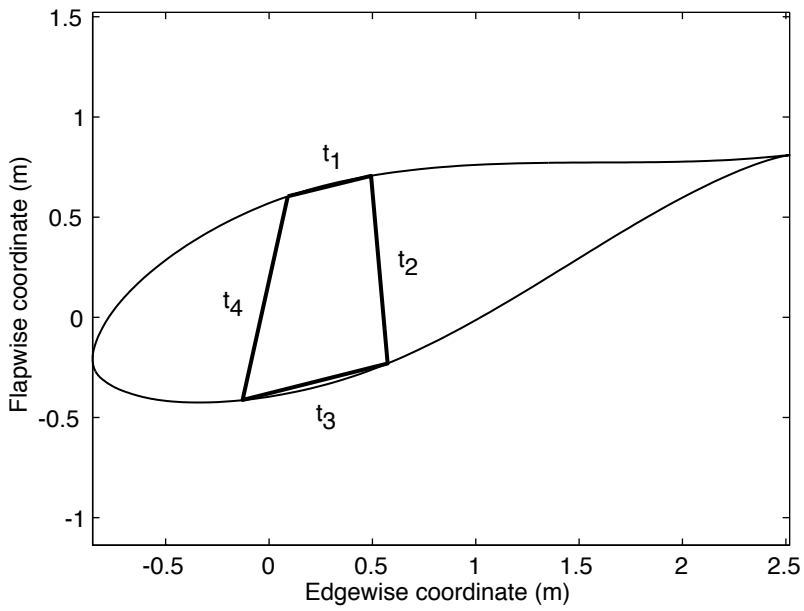
(b) Mass $= 122.46\,\mathrm{kg/m}$

Figure 6: Comparison between best spar's section design at a fixed radial coordinate (10 metres) considering conventional (a) and adaptive (b) designs
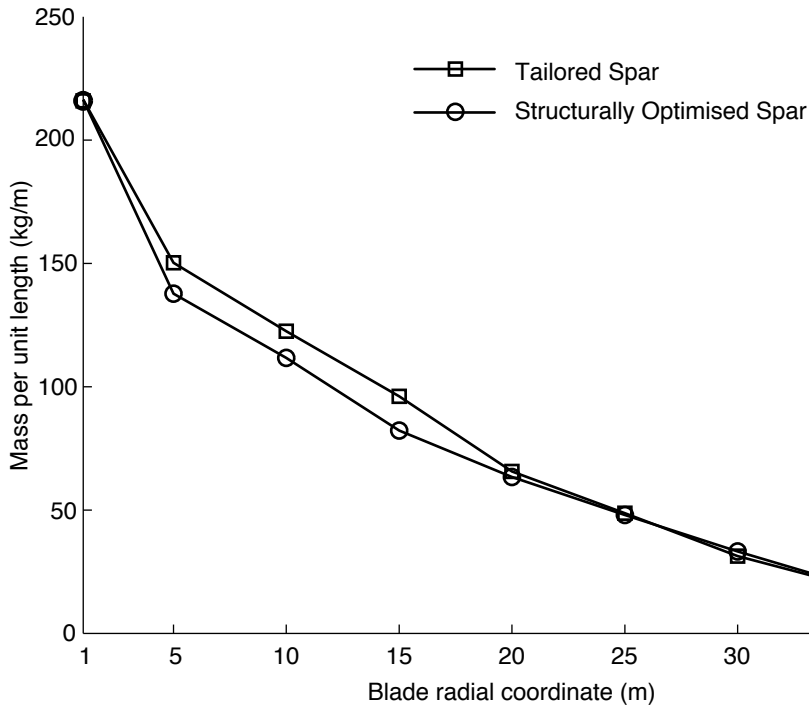
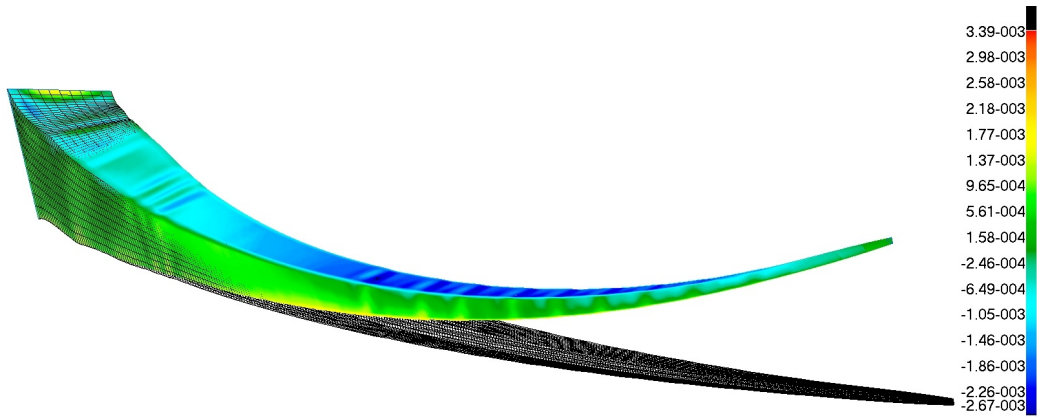Figure 7: Distribution of minimum mass per unit length along the radial coordinate

Figure 8: Distribution of direct axial strain along the spar radial coordinate, optimised adaptive spar
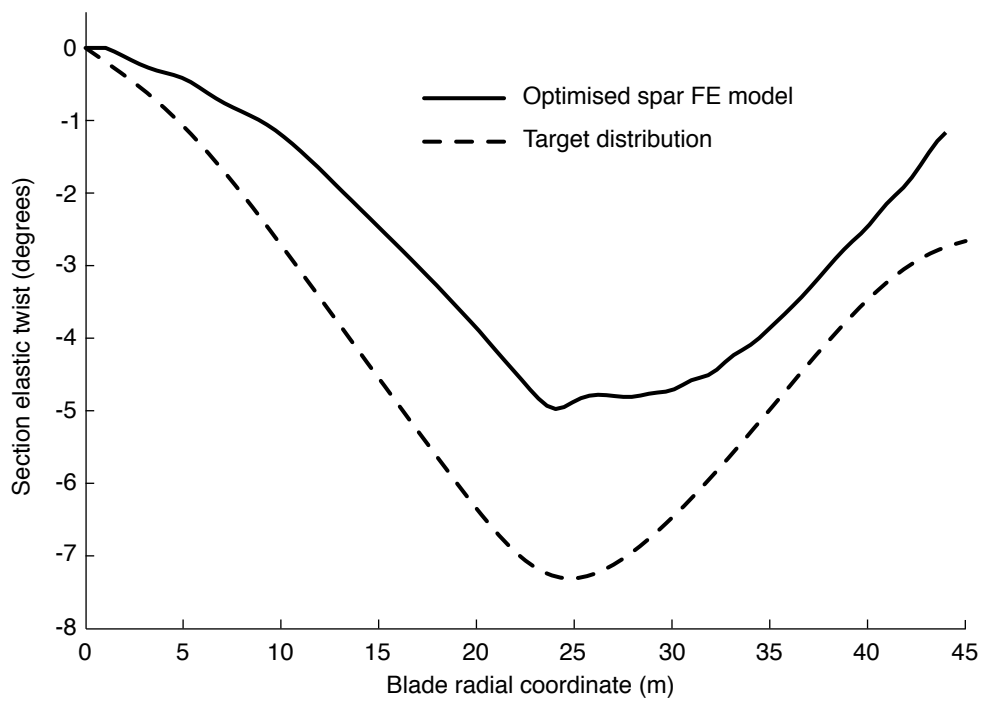
Figure 9: Distribution of induced elastic twist under rated aerodynamic load, FE analysis results for the optimised adaptive structure

elastic twist, shown as the dashed line in figure 9, should be included in the optimisation algorithm.

In conclusion, it has been shown that (a) it is possible to design the adaptive behaviour into a realistic spar model and (b) the weight penalty due to required stiffness tailoring is marginal and approximately 5%. In the remainder of our study, the focus extends to complete blades.

3. Design of the adaptive behaviour into a complete blade structure

The feasibility of the adaptive concept identified in [7, 8] is now evaluated by considering complete WT blades with a spar-plus-skin structural configuration. By adding external skins, the flapwise bending stiffness increases slightly, but twist and edgewise bending stiffnesses become significantly greater. Therefore, as the adaptive concept relies on exploitation of bend-twist coupling, the spar design requires modification, reflecting the changes in the overall structural geometry. As such, quantitative improvements in performance are re-evaluated. This section discusses the driving features and constraints for the design of the adaptive blade. Geometric nonlinear effects are also investigated and a modal analysis is undertaken to assess the effects of elastic tailoring on the structural dynamics of the blade.

An extreme flapwise bending load, identical to that of section 2, is used as an input for the current analysis. In addition, a reverse flapwise and two edgewise load cases are considered. The reverse flapwise case which, by definition, brings tension over the suction side of the blade, is obtained by changing the sign of the forward load and by scaling it by 0.75 (note, 0.75 is the scale factor applied to the extreme forward flapwise load; thus, the reverse case scales up the rated aerodynamic load by a factor of -1.125). The edgewise loads, both forward and reverse, are obtained from the reference blade's load envelope and correspond to those used in [11]. A forward edgewise load causes compression over the blade's trailing edge, whilst the opposite holds for a reverse edgewise case. The structural constraints, relative to each load case, are the same as those considered in section 2. Strength and buckling limits, a minimum number of zero degree plies in all of the laminates (to ensure a load path) and a maximum flapwise displacement for tower clearance are thus imposed.

The full blade's FE model (shown in figure 10) comprises four walls for the spar box plus one panel for the leading edge and two panels for the trail-

Figure 10: Finite Element model, full blade structure

ing edge, i.e. upper and bottom panels. At a given cross section, all seven panels have a constant thickness, which varies spanwise. The full FE model uses the same elements and properties as described in section 2. However, the mesh along airfoil profiles is significantly refined. The final converged mesh presents 202 segments along airfoil sections, plus 6 segments for each web. The node distribution is refined in higher curvature regions. Sandwich panels are used for the TE and the LE. These are modelled with thick sandwich laminates whose core is made of a medium-density foam (isotropic material with $100\,\mathrm{MPa}$ Young's modulus, Poisson's ratio $= 0.3$ and density of $100\,\mathrm{kg/m^3}$). The external plies of the sandwich construction are made of the same CFRP used for caps and webs (see Table 1 for material properties).

3.1. Functional design

The blade described so far has not been optimised in a robust way but does deliver a working design. As a consequence, the thicknesses are not minimised and do not necessarily maximise safety factors against structural constraints. The structural optimisation of the adaptive blade can be considered as a further development of this research, but is beyond current aims.

Here, the aerodynamic profile of the blade is the same as that of the reference. The planform geometry is set to have the same axis of the swept spar, described in section 2.1. The three-dimensional geometry is defined
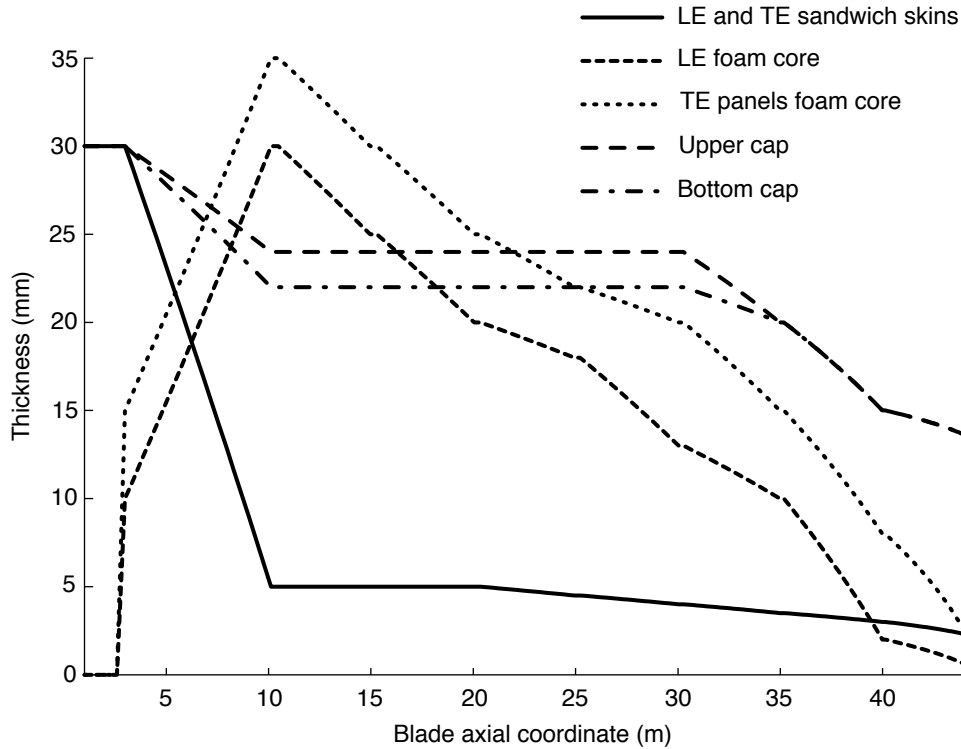
15

Figure 11: Distribution of section's laminates thickness along the blade radial coordinate

from the shape of the curved axis, as discussed in section 2.1. However, edgewise translations of cross sections bring their quarter-chord location, rather than their centre, onto the curved axis. Similarly, the cross sections are rotated around the quarter-chord, rather than around the centre.

The final design comprises a composite spar, in which 90% of plies have an aeroelastically tailored orientation. The skins of the TE and LE sandwich panels are also tailored (80% of the thickness). The remaining thickness is made up of 10% of 90 degrees plies, 40% of ±45 and 50% of 0 degree plies. The webs' lay-up is not aeroelastically tailored. Figure 11 shows the distribution of the panel thickness along the blade axis. The first three metres of span are relatively thick-walled (note, the cross section is almost cylindrical at this span location). In this area, sandwich panels are not used, i.e. zero thickness of the core. Further outboard, thick panels in the TE and LE regions are gradually replaced with sandwiches. Sections outboard of 10 metres have thick caps and sandwich construction over TE and LE regions. From this
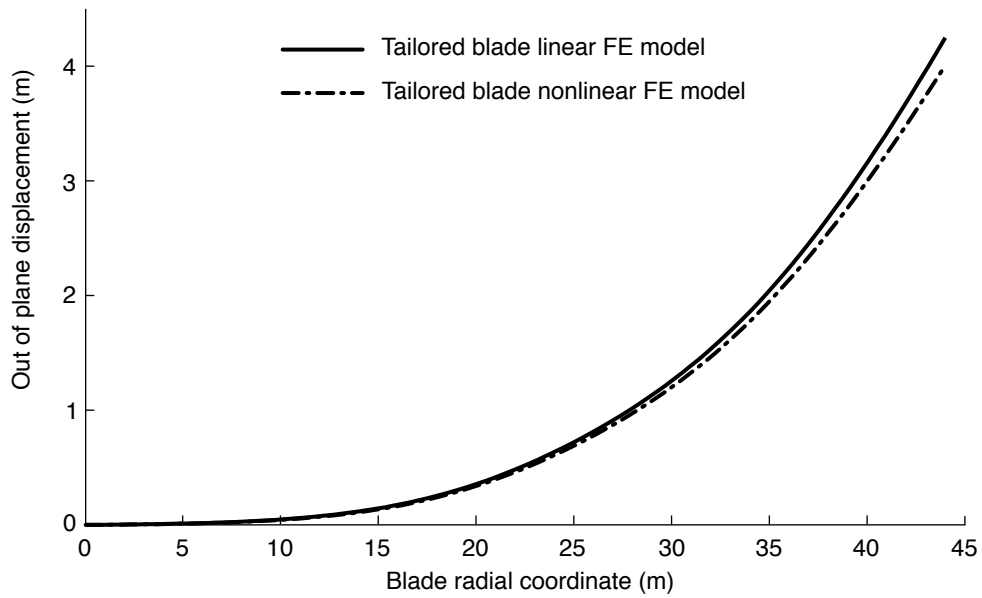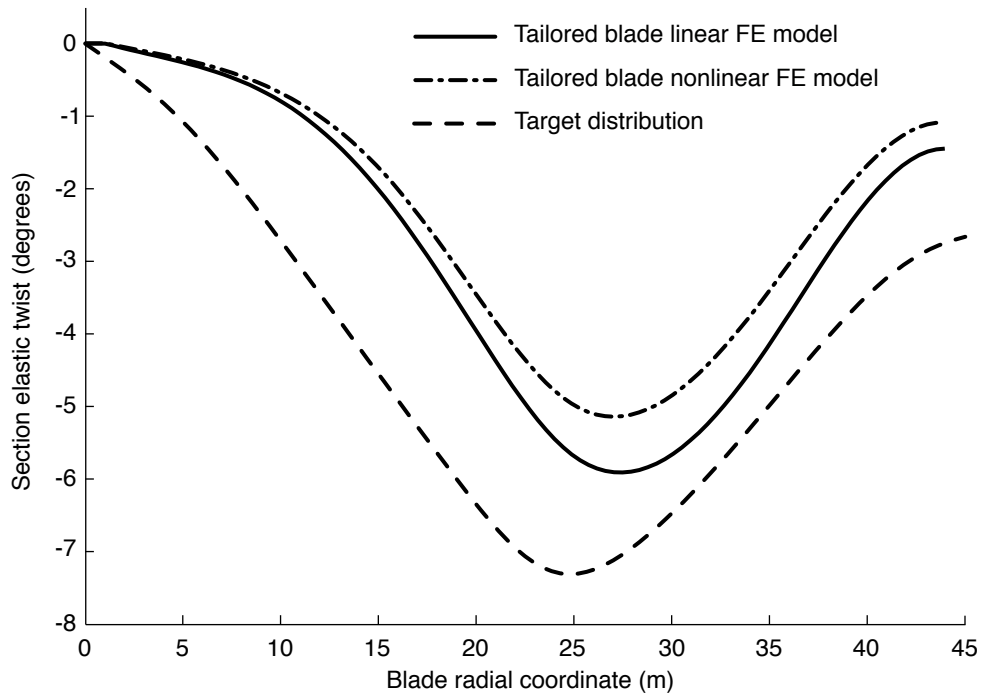
16

Figure 12: Distribution of induced elastic twist and out-of-plane displacement under rated aerodynamic load, fully tailored blade design

17

position outward all of the laminates' thicknesses decrease slightly, with the exception of the cores' thickness that decreases more prominently.

Figure 12 shows that the intended distribution of the induced twist is realized by this design. Nevertheless, the maximum amount of twist is roughly one degree less than in the targeted distribution. Also, its location is slightly repositioned outboard along the radial direction. This modification to the passive adaptive behaviour does not affect the power performance of the adaptive blade, but it can reduce the load alleviation capability. Further details are given in section 3.4.

Figures 13 and 14 show the strain distribution on the outermost ply of the blade when the extreme flapwise load is applied. In the current model, tow steered plies are placed externally, while the middle part of the stack is made of conventional ply orientations. Figure 14 shows that the in-plane shear strain reaches the allowable value over some regions of the blade. Similar observations hold for the direct axial strain in the zero degree plies (which are not shown because they are located within the laminate's thickness). In general, these figures show the effect of stiffness tailoring in terms of strain distributions. Indeed, for the external ply, larger direct strains are located over the blade's mid-span section (see figure 13), because here the tows are mainly oriented parallel to the structural axis. On the other hand, maximum values of shear are located before and after the maximum direct strain region (see figure 14). In fact, over these sections the level of fibre steering with respect to the blade axis is the greatest. For completeness, the absolute maximum values of direct and in-plane shear strain (reported in table 2) occur at one-third of the blade length from the root. In particular, the maximum direct strain is found on the bottom spar cap at the 25th ply from the outer surface. The maximum in-plane shear is located on the outermost ply of the trailing edge panel on the pressure (bottom) surface of the airfoil, towards the spar cap.

Extreme flapwise bending is usually a driving load case, particularly for strength limits in the caps and buckling in the TE laminates. Figure 15 shows the first buckling mode under flapwise bending. The corresponding buckling safety factor is equal to 1.04. Buckling, in this case, takes place over the upper TE laminate, close to the quarter-span section. The reverse flapwise load provides a buckling safety factor of 1.16 and, on average, strains which are slightly smaller than in the forward case. Edgewise loads are not critical. The induced strains are relatively small and the lowest buckling safety factor equals 1.95. This instability takes place over the blade's LE, because it is
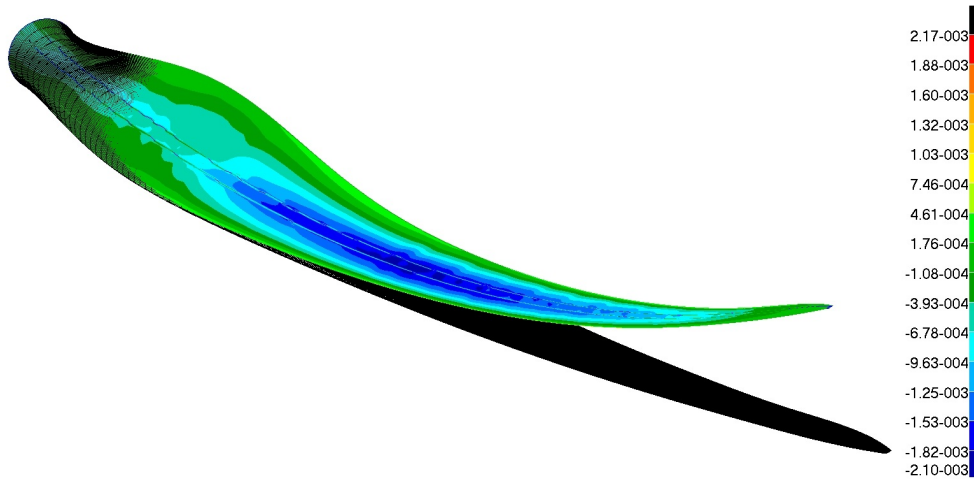
Figure 13: Distribution of direct strain under extreme flapwise load for the final adaptive design

obtained under a reverse edgewise load.

These results confirm that the targeted adaptive behaviour is achievable with realistic blade geometries. However, the final structural assembly, i.e. spar plus skin, is much stiffer in torsion. Therefore, the maximum values of induced twist decrease, but remain significant from an aerodynamic perspective. This point is discussed in more depth in section 3.4.

3.2. Nonlinear analysis

The effects of geometric nonlinearities on the blade's deformation mechanisms are now assessed. The design process has been hitherto based upon linear elastic analyses. Nevertheless, under flapwise loading, the magnitude of the displacements is relatively large, so nonlinearities may arise. Furthermore, previous studies [12] have shown that the Brazier effect, i.e. localised bending of cross-sectional panels, can be significant. Consequently, its influence on structural strength should be investigated.

Nonlinear analyses are performed by means of MSC NASTRAN's solver 106 and using the mesh described in section 3. The deflection at rated wind speed is shown in figure 12. By comparison of the linear and nonlinear responses, the geometric nonlinearity is observed to stiffen the blade. The distribution of induced elastic twist is not qualitatively modified. Nonetheless, twist values are decreased, following the reduction of the out-of-plane displacements. The stiffening effect is also clearly observed under extreme
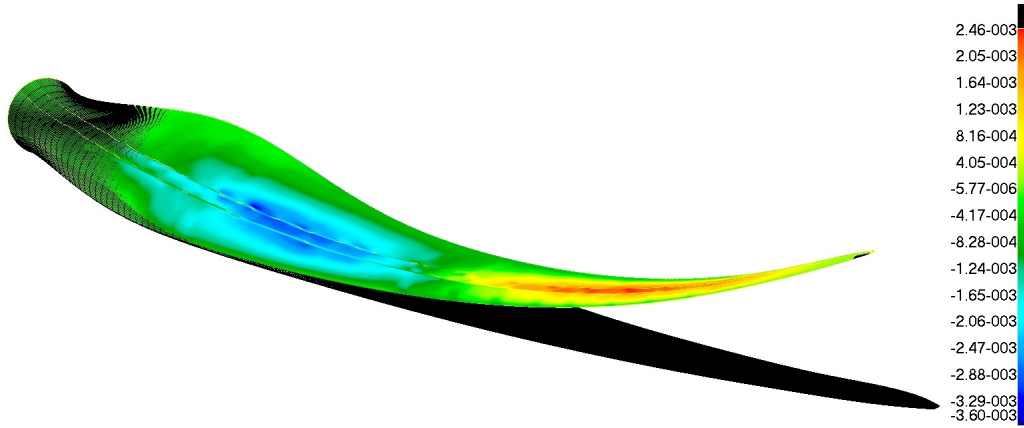
19

Figure 14: Distribution of in-plane shear strain under extreme flapwise load for the final adaptive design

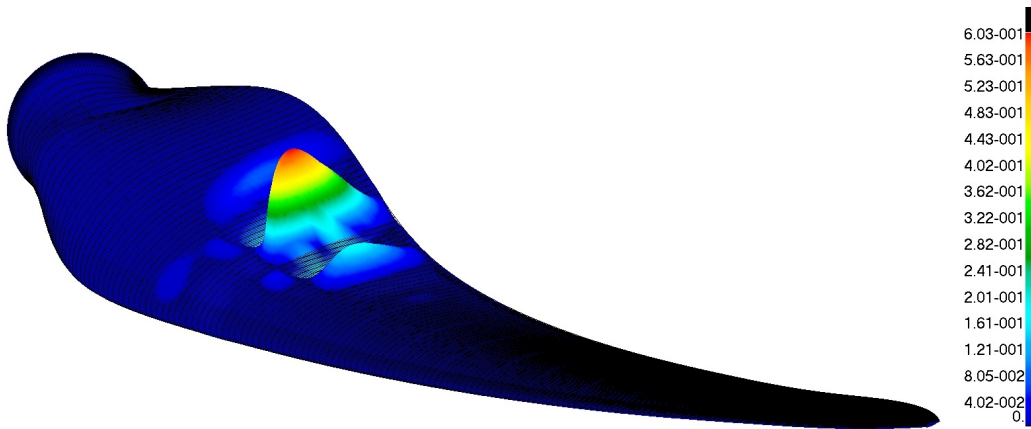Figure 15: First buckling mode under extreme flapwise load for the final adaptive design

Table 2: Comparison between linear and nonlinear results, design constraints

Max values in	Flapwise displacement [m]	Direct strain [μstrain]	In-plane shear [μstrain]
Linear Analysis	6.99	3600	3600
Nonlinear Analysis	6.56	3300	3430
Variation (%)	6.15	8.3	4.7

Table 3: Adaptive blade, lowest natural frequency

Mode number [−]	Mode frequency [Hz]
1	1.276
2	2.953
3	3.832
4	7.208
5	8.484

flapwise bending.

Table 2 shows a comparison between linear and nonlinear results. Non-linearities under edgewise bending are found to be negligible and are not shown. In addition, the Brazier effect does not increase the strain on the webs significantly and can thus be neglected. The comparison highlights the potential for reducing the structural weight by taking into account effects of nonlinear stiffening. As already mentioned, nonlinear stiffening on flapwise bending decreases induced twist angles. However, values similar to those produced by linear analysis, can be obtained by reducing skin thicknesses, with the additional benefit of decreasing weight.

In conclusion, nonlinear effects play an important role in the out-of-plane deformation of the blade, but linear analyses are generally conservative and are suitable for a first approach for this design. Nonetheless, there is potential to lighten the structure via nonlinear design methods, as long as the Brazier effect is negligible.

3.3. Modal analysis

To complete the current study, a modal analysis is performed on the adaptive blade. Modal features are calculated with reference to the stationary blade, thus excluding rotational effects. The effect of the adaptive capability on modal shapes and on values of natural frequencies is analysed with MSC NASTRAN's solver 103 and by using the mesh described in section 3.

As a simple general rule for design, the two lowest natural frequencies of the blade are compared to the rotational frequencies of the WT (see [13]). A sufficient margin of safety to these frequencies avoids blade resonance. Specifically, the natural frequencies should not lie within the rotational frequency $\mp 12\%$. In the current study, the operating angular speed of the reference WT varies between 0.15 and 0.25 Hz. Table 3 shows the lowest five natural
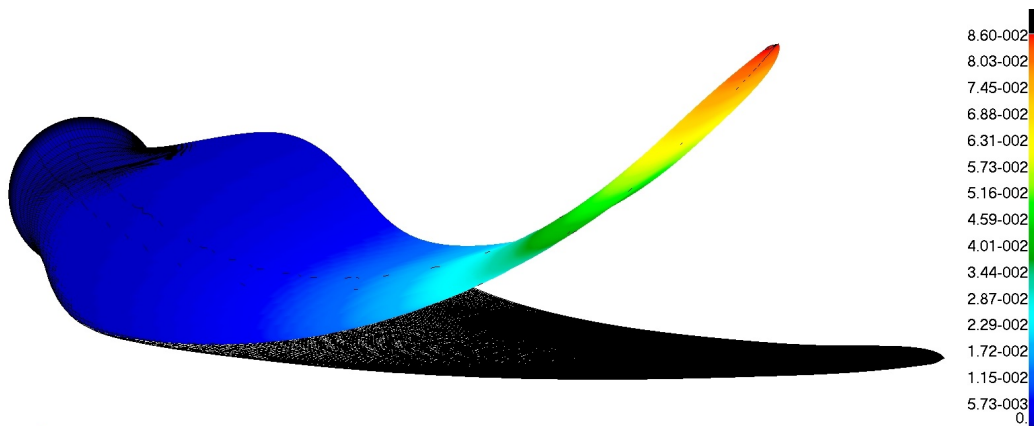
Figure 16: First modal shape for the adaptive blade design, natural frequency equal to 1.276 Hz

frequencies of the blade. Figure 16 shows the first modal shape. These results show that blade resonance at low frequency is not a concern. However, the natural frequencies and, in particular, those associated with flapwise bending modes do change as a function of the rotational dynamics. This aspect should, therefore, be investigated further.

Figures 17 and 18 show the first two natural mode shapes. As expected, each mode excites different degrees of freedom (DOFs) simultaneously. In fact, out-of-plane displacements and twist angles are strongly coupled by design. Of particular interest is the fact that the second modal shape shows a nose-up bend-twist coupling that could detrimentally affect the aeroelastic response of the structure to gusts, relative to loads in a range of frequency close to 2.95 Hz. Nevertheless, blade rotation could modify these dynamic features significantly.

In summary, this modal analysis shows that the natural frequencies of the adaptive blade are positioned appropriately with respect to the operating angular speeds of the turbine. In addition, modal shapes do show anticipated features, i.e. strongly coupled responses. Some modal shapes show a nose-up bend-twist coupling and thus their effect (modal participation) on the blade's gust response calls for future investigation.

3.4. Remarks about the power performance of the adaptive blade

References [7, 8] showed that, by changing the sign of the slope of the elastically-induced twist distribution over the outer half of a blade, the load
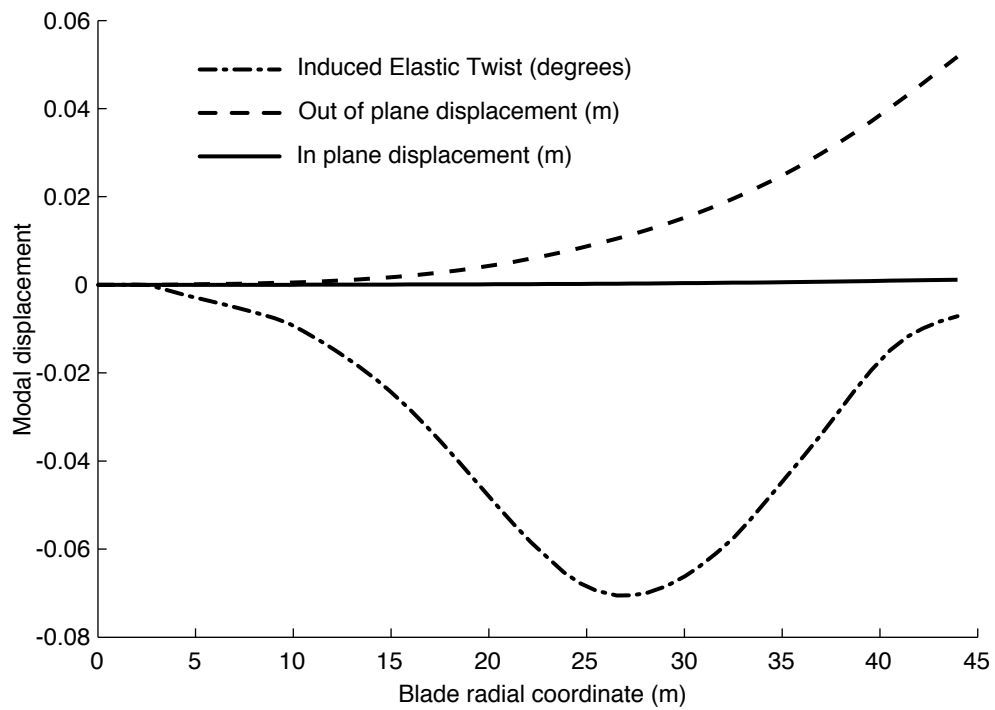
Figure 17: First modal shape for the adaptive blade design, distributions of the section DOFs along the blade axis
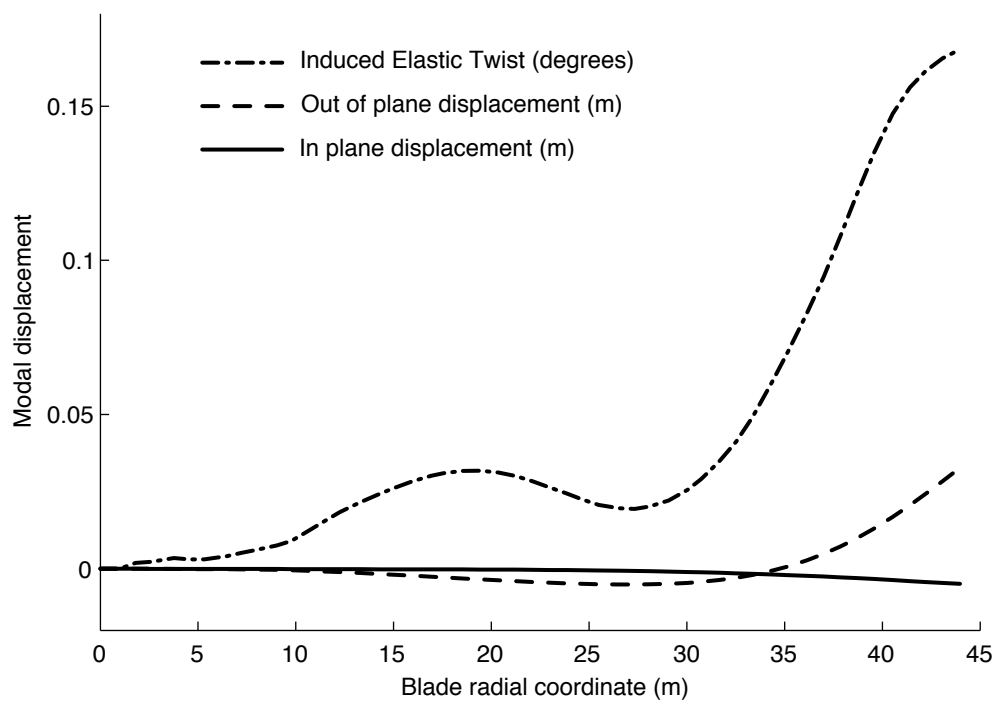
Figure 18: Second modal shape for the adaptive blade design, distributions of the section DOFs along the blade axis

alleviation capability typical of nose-down coupled blades can be retained, while simultaneously improving the power harvesting performance. The latter point is novel and differentiates the aeroelastic concept presented here from previous works on pitch controlled WTs in which the nose-down coupling entailed a decrease of Annual Energy Production (AEP) [4].

The distribution of elastically-induced twist required to achieve these results is indicated in figure 1 and changes from 0 at the root to approximately 7 deg at the mid-section to 3 deg at the blade tip. Power calculations show that this passive deformation increases the power yielded when compared to conventional, uncoupled blades. However, section 3.1 shows that a decrease of the minimum twist value may be necessary to satisfy structural constraints. This effect corresponds practically to a shift upward of the curve in figure 1, over its outermost half.

We have calculated that this modification does not affect the power performance of the adaptive blade, but it suggests a change to the pitching angles at different wind speeds and has the potential to decrease the gust load alleviation capability. The improvement of AEP is mainly driven by the difference of induced twist between the blade's mid-span and tip sections and less related to absolute values. This behaviour arises because a wind speed increase requires a differential twist variation in order to follow the aerodynamic twist that maximises power. This variation should increase the total twist of inboard sections more than outboard. Consequently, if the targeted distribution is translated (figure 1) and the pitch value simultaneously changed to compensate for this translation, the power curve would not be modified (apart from negligible aeroelastic effects). However, the nose-down rotation of the blade's sections would decrease, on average, and this should reduce the gust load alleviation.

4. Concluding remarks and future work

This study confirms numerically that the adaptive behaviour identified in [7, 8] can be engineered into a complete wind turbine blade. This has been done by means of finite element models of the full blade structure and with realistic load cases and constraints. The functional example of the adaptive blade achieves the targeted passive behaviour and fulfils design constraints. Nevertheless, its design is not structurally optimised.

In section 2.2 the weight penalty due to elastic tailoring of the spar was assessed. This penalty was found to be approximately 5% of the weight of

the structurally optimised spar, which is not aeroelastically tailored. This value is expected to be an upper bound, because load reductions due to aeroelastic tailoring have not been included in the structural optimisation studies. It is also worth noting that the weight penalty mainly affects the spar. Indeed, during extreme load conditions, the remaining part of the structure is not highly loaded, and more importantly, is not close to critical strength conditions. Thus, the mass penalty is not expected to be greater that 5% for the complete blade.

In general, tower clearance is not a driving constraint for the adaptive design. Conversely, flapwise loads are critical both for strength over spar caps and buckling over TE laminates. Edgewise loads can be critical for local buckling on LE and TE panels.

Section 3.2 considers the effect of geometric nonlinearities. In the case considered, linear analyses were found to be conservative for design purposes.

Future development could include a structural optimisation of the full blade. In particular, a multi-objective and multi-physics approach would allow both structural and aeroelastic objectives to be included in the study—two important considerations when aeroelastic tailoring is involved. The structural optimisation should be complemented with gust response analyses, to assess the load alleviation capability of this adaptive blade concept.

Furthermore, other design solutions remain to be investigated. For example, the viability of a blade design with only one web is an interesting alternative to be studied. Indeed, this solution can significantly increase the twist flexibility, and thus the magnitude, of the elastically-induced twist. Load cases considering certification should be considered, as well as fatigue life assessment. In principle, the adaptive behaviour should enhance fatigue issues by reducing load oscillations due to gust and turbulence. On the other hand, the use of unbalanced laminates and tow steering can modify the strength of the material and introduce manufacturing-induced defects. Therefore, further studies on fatigue phenomena are recommended. The variation of natural frequencies, due to elastic tailoring, should also be analysed and related to frequency of self-weight, inertial and aerodynamic loads (e.g. wind shear).

Appendix A. Efficient curved blade, aerodynamic considerations

Aerodynamic models for rotors, such as the blade element momentum (BEM) theory, are based upon the aerodynamics of 2D sections. In the

case of curved blades, these methods consider the flow to be two-dimensional and perpendicular to the blade axis. For instance, this approach is used in [1] and [14] to develop the aerodynamic analysis of swept WT blades. As a consequence, the three dimensional geometry of the blade is obtained by moving the airfoils' quarter-chord points onto the swept axis and then rotating them so that they align perpendicularly to the axis.

This project, as explained in section 3.1, takes a different approach. Starting from the swept axis and the 3D shape of the straight blade, each section is first translated perpendicularly to the radial coordinate. This translation moves the sections' quarter-chord onto the curved axis. Then, the section is rotated inside the rotor plane so that the profile becomes perpendicular to the vector joining the quarter-chord and the rotor centre.

With this arrangement the aerodynamic profiles are not (necessarily) perpendicular to the blade axis, but align with the plane in which the flow is actually two dimensional. In fact, by combining the wind speed and the rotational speed, the flow vector for the swept blade is perpendicular to the position vector, not to the swept axis direction. Consequently, in order to apply the 2D flow approximation to our curved geometry, the flow does not need to be decomposed into the parts parallel and orthogonal to the blade axis. The flow is simply two-dimensional over the blade's aerodynamic cross-section.

Decomposing the flow vector or, equivalently, projecting it onto the direction perpendicular to the curved axis, would reduce the local dynamic pressure and, in turn, decrease the aerodynamic force and the torque on the rotor. Conversely, by using our swept geometry, the projection of the lift onto the rotor plane is beneficial for power generation, because it lies perpendicular to the section position vector, which then coincides with the arm of the force. By using the approach adopted in [1] and [14], i.e. when the aerodynamic section is perpendicular to the blade axis, the lift has a component in the rotor plane that lies parallel to the arm does not generate torque.

These assertions are based upon simple aerodynamic considerations and should be validated against more refined aerodynamic analysis, i.e. three dimensional CFD of the whole turbine. However, their validity does not influence the potential of the adaptive concept introduced herein. Indeed, as our focus was on power gain due to the structural adaptive capability, rather than on the effects of different planforms, the blade has been modelled as being approximately straight aerodynamically.

Acknowledgments

The authors wish to thank Chris Payne and Tomas Vronsky of Vestas Technology R&D for their technical support.

References

[1] Liebst BS. Wind turbine gust load alleviation utilizing curved blades. Journal of Propulsion 1986;2(4):371–7.

[2] Veers PS, Lobitz DW, Bir G. Aeroelastic tailoring in wind-turbine blade applications. Tech. Rep.; Sandia National Labs; 1998.

[3] Lobitz DW, Veers PS. Aeroelastic behavior of twist-coupled HAWT blades. In: Aerospace Sciences Meeting and Exhibit, 36th, and 1998 ASME Wind Energy Symposium, Reno, NV, Jan. 12-15, 1998, Collection of Technical Papers (A98-16844 03-44). 1998,.

[4] Lobitz DW, Laino DJ. Load mitigation with twist-coupled HAWT blades. In: Aerospace Sciences Meeting and Exhibit, 37th, and 1999 ASME Wind Energy Symposium, Reno, NV, Jan. 11-14, 1999, Collection of Technical Papers (A99-17151 03-44). 1999,.

[5] Zuteck MD. Adaptive blade concept assessment: Curved platform induced twist investigation. Tech. Rep.; Sandia National Labs; 2002.

[6] Larwood S, Zuteck M. Swept wind turbine blade aeroelastic modeling for loads and dynamic behavior. AWEA Windpower 2006, Pittsburgh, PA, June 4-7; 2006.

[7] Capuzzi M, Pirrera A, Weaver PM. A novel adaptive blade concept for large-scale wind turbines. Part I: Aeroelastic behaviour. Energy 2014;73:15–24.

[8] Capuzzi M, Pirrera A, Weaver PM. A novel adaptive blade concept for large-scale wind turbines. Part II: Structural design and power performance. Energy 2014;73:25–32.

[9] Cooper AAG. Trajectorial fiber reinforcement of composite structures. Ph.D. thesis; Washington University, St. Louis, Missouri; 1972.

[10] Librescu L, Song O. On the static aeroelastic tailoring of composite air-craft swept wings modelled as thin-walled beam structures. Composites Engineering 1992;2(5–7):497–512.

[11] Pirrera A, Capuzzi M, Buckney N, Weaver PM. Optimization of wind turbine blade spars. 53rd AIAA/ASME/ASCE/AHS/ASC Structures, Structural Dynamics, and Materials Conference, 23-26 April 2012, Honolulu, Hawaii, AIAA Paper 2012-1500; 2012.

[12] Jensen F, Weaver P, Cecchini L, Stang H, Nielsen R. The brazier effect in wind turbine blades and its influence on design. Wind Energy 2012;15(2):319–33.

[13] Guidelines for Design of Wind Turbines, 2nd Edition. DNV/Risø; 2002.

[14] Larwood SM. Dynamic analysis tool development for advanced geometry wind turbine blades. Ph.D. thesis; Mechanical and Aeronautical Engineering, Office of Graduate Studies of the University of California; 2009.